17th International Congress of the Geological Society of Greece

28-31 May, 2025 - Mytilene, Greece

Bulletin of the Geological Society of Greece, Sp. Publ.

Ext. Abs. 00000

Application of a machine-learning model for the determination of focal mechanisms in the area of the Corinth Rift Laboratory Near-Fault Observatory (CRL NFO), Central Greece

Kapetanidis V.[1], Spingos I.[1], Kaltsas, C.[1], Kaviris G.[1]

(1) National and Kapodistrian University of Athens, Section of Geophysics-Geothermy, Seismological Laboratory, Athens, Greece, vkapetan@geol.uoa.gr

Research Highlights

- First motion polarities determined using an ML model yielded results comparable with manual measurements.
- Discrepancies were mainly observed at stations in larger epicentral distances or equipped with accelerometers.

Introduction

The large quantities of seismic waveform data available have rendered their manual analysis a challenging task. The unification of seismic networks in Greece (e.g., Evangelidis et al., 2021) has improved the completeness of the seismic catalogs provided by routine analysis. However, as the number of earthquakes is multiplied almost tenfold for every lowering of magnitude by a unit, manual analysis can only go so far before the workload becomes prohibiting. Conventional automatic seismic P- and S-wave arrival-time picking methods also have downsides, depending on the objective function used in each case. Despite providing quick solutions, the measurements of these automatic methods are usually less accurate than those performed by human analysts, and they need to be manually revised for their quality to be improved. However, in recent years, the rise of Machine-Learning (ML) models has revolutionized the automatic processing of seismological data. ML models, such as PhaseNet (Zhu & Beroza, 2019) and EQTransformer (Mousavi et al., 2020), are now used for the automatic analysis of huge datasets, greatly augmenting the number of detected events and lowering the completeness magnitude of seismic catalogs. Even more surprisingly, in terms of accuracy, these ML methods provide results that are on par with manually analyzed data (e.g., Mousavi et al., 2020), and can even recognize P- and S-wave arrivals in noisy signals without the application of a filter (e.g., Zhu & Beroza, 2019).

An even more challenging task is the automatic measurement of P-wave First Motion Polarities (FMPs). For events of moderate or higher magnitude (e.g., M≥3.6), the focal mechanisms can usually be determined through moment tensor inversion, by fitting synthetic waveforms to the observed ones. FMPs, on the other hand, are useful for determining focal mechanisms for weak-magnitude events (M≤3.5), particularly when a local network is available near the epicentral area. FMPs depend on the radiation pattern of seismic energy at an earthquake's focus. In the double-couple model, FMPs are distributed in four quadrants, characterized by the alternating sign of the first motion recorded at the vertical component of the seismic stations. These first pulses can be impulsive or emergent, which depends on the angle of emergence of the seismic ray at the focus, relative to the radiation pattern of the earthquake, which in turn depends on the focal mechanism; i.e., the strike, dip, and rake of the source. Rays originating near the P or T principal axes of the moment tensor are expected to produce impulsive negative or positive first motions, respectively. On the other hand, rays originating near the nodal planes or the null axis are likely to produce emergent first motions, which cannot be easily distinguished. Furthermore, the Signal-to-Noise Ratio (SNR) of weak-magnitude events can be too low for even a P-wave arrival to be picked. The application of filters to lower the noise level and improve SNR can distort the first pulse and lead to an erroneous FMP measurement. Even when a P-wave arrival-time can be roughly assessed, the analyst must decide whether to characterize the polarity of the first motion or skip it to avoid an error. Other measurements that can help constrain the focal mechanisms of weak events include the S-to-P amplitude ratio and the S-wave polarization direction (e.g., Kapetanidis et al., 2015).

As the characterization of the FMP is a pattern recognition task, it has also been the subject of studies employing methods based on artificial intelligence. Such ML models can recognize these patterns and classify the first pulse as being positive or negative, assess whether it is impulsive or emergent, or decide to dismiss a measurement if the polarity cannot be safely determined. Examples of such ML models include those presented by Ross et al. (2018) and Zhao et al. (2023). Both models were trained on a large dataset of seismic waveforms from Southern California, and the authors reported a precision of ~95% or more compared to the respective FMP measurements by human analysts.

Background

The Corinth Rift Laboratory is a local seismological network that has been established in the Western Gulf of Corinth (WGoC; Figure 1) since the early 2000s (Chiaraluce et al., 2022). It is one of the Near-Fault Observatories (NFOs) of the European Plate Observing System (EPOS), complemented by stations of the regional Hellenic Unified Seismic

Network (HUSN). WGoC is one of the most seismically active areas in Greece, due to a high extension rate, reaching ~16 mm/yr in a ~N-S direction (Avallone et al., 2004), mainly characterized by E-W normal faulting. Between December 2020 and February 2021, an intense seismic swarm occurred in WGoC (Kaviris et al., 2021; Serpetsidaki et al., 2023). The swarm mainly evolved in three phases, each triggered by a significant earthquake: an M_w=4.6 event on 23 December 2020 near Marathias; an M_w=5.0 event on 12 January 2021 near Trizonia Island; and an M_w=5.3 event on 17 February 2021 (Zahradník et al., 2022), north of Psathopyrgos. An examination of the aftermath period up to December 2022, showed that the swarm activity diminished after March 2021, and a background seismicity level was established, with only a few spatiotemporal clusters and two significant earthquakes of M_w=4.2 and M_w=4.3, on 30 November 2021 and 29 July 2022, respectively (Kaltsas et al., 2024). In the framework of the studies of Serpetsidaki et al. (2023) and Kaltsas et al. (2024), a total of 117 focal mechanisms were calculated between December 2020 and December 2022, with 20 from the former study being assessed through moment tensor inversion, while the rest were determined using P-wave first motion polarities. Most focal mechanisms indicate normal faulting, with a smaller proportion of strike-slip or oblique-normal events also being detected.

Figure 1. The Western Gulf of Corinth (WGoC) in Central Greece. Seismological and accelerometric stations of the Corinth Rift Laboratory Near-Fault Observatory (CRL-NFO) are depicted as triangles. The focal mechanisms of selected significant earthquakes of the period December 2020 – December 2022 are presented with beachball symbols. The relocated seismicity of the period December 2020 – February 2021 (gray circles) is after Serpetsidaki et al. (2023). The fault lines are from the NOAfaults database (Ganas et al., 2013).

Objectives

In this work, we apply a machine-learning model to measure the FMPs and determine the focal mechanisms of earthquakes that occurred between December 2020 and December 2022 in the western Gulf of Corinth. This will provide a perspective on the efficiency and accuracy of the applied model with the abovementioned dataset, as there are also available manually measured FMPs for a subset of the events that will be processed. The latter will be used to examine the validity of the FMPs, but also to measure the difference in the resulting focal mechanisms derived from the herein-applied method compared to previous results of manually measured FMPs.

Data and Methods

We use a catalog of ~460 manually analyzed and relocated events from the seismic crisis in WGoC between December 2020 and February 2021 (Serpetsidaki et al., 2023), as well as 82 events from the aftermath period between March 2021 and December 2022 (Kaltsas et al., 2024); the selected events have M≥2.0. In both cases, there is a subset of events with available manually measured FMPs and calculated focal mechanisms with a grid-search method, that will be used for comparison. We acquire seismic waveform data from the EIDA nodes of Reseau Sismologique et Geodesique Francais (RESIF; https://seismology.resif.fr/eida/), for stations of the CRL network, and the National Observatory of Athens – Geodynamics Institute (NOA-GI; http://eida.gein.noa.gr/webdc3/), for stations of HUSN.

We employ the DiTing-Motion (DTM) machine-learning model (Zhao et al., 2023) to automatically measure the FMPs at local stations in the area of WGoC. For each station, the waveform recording of the vertical component is detrended, resampled to 100 sps, if necessary (e.g., for accelerometric stations, which are usually at 200 sps), and cropped to a 128-sample window of ±0.64 s around the arrival-time of the P-wave. We follow the workflow established by Zhao et al.

(2023), also measuring the S-to-P amplitude ratio (SPR) and employing the HASH code (Hardebeck & Shearer, 2002, 2003) to determine the focal mechanisms using both FMPs and SPR. To assess the influence of the P-wave's arrival-time accuracy on FMP measurements, we also test the procedure after re-picking the P-wave in the vicinity of the previously available arrival-time with Phasenet, pre-trained with data from the INSTANCE dataset (Michelini et al., 2021). We examine DTM results in terms of FMP measurement accuracy, compared to manually analyzed events, both automatically and by visually reviewing the automatic FMP measurements (Figure 2, left). The discrepancies are also examined on a per-station level to identify any systematic issues related to particular stations. For the difference between the new focal mechanisms and the previously available ones from the common subset, we measure the Kagan angle between the two solutions and also examine the whole image of their beachball projections on the map for visible similarities or differences.

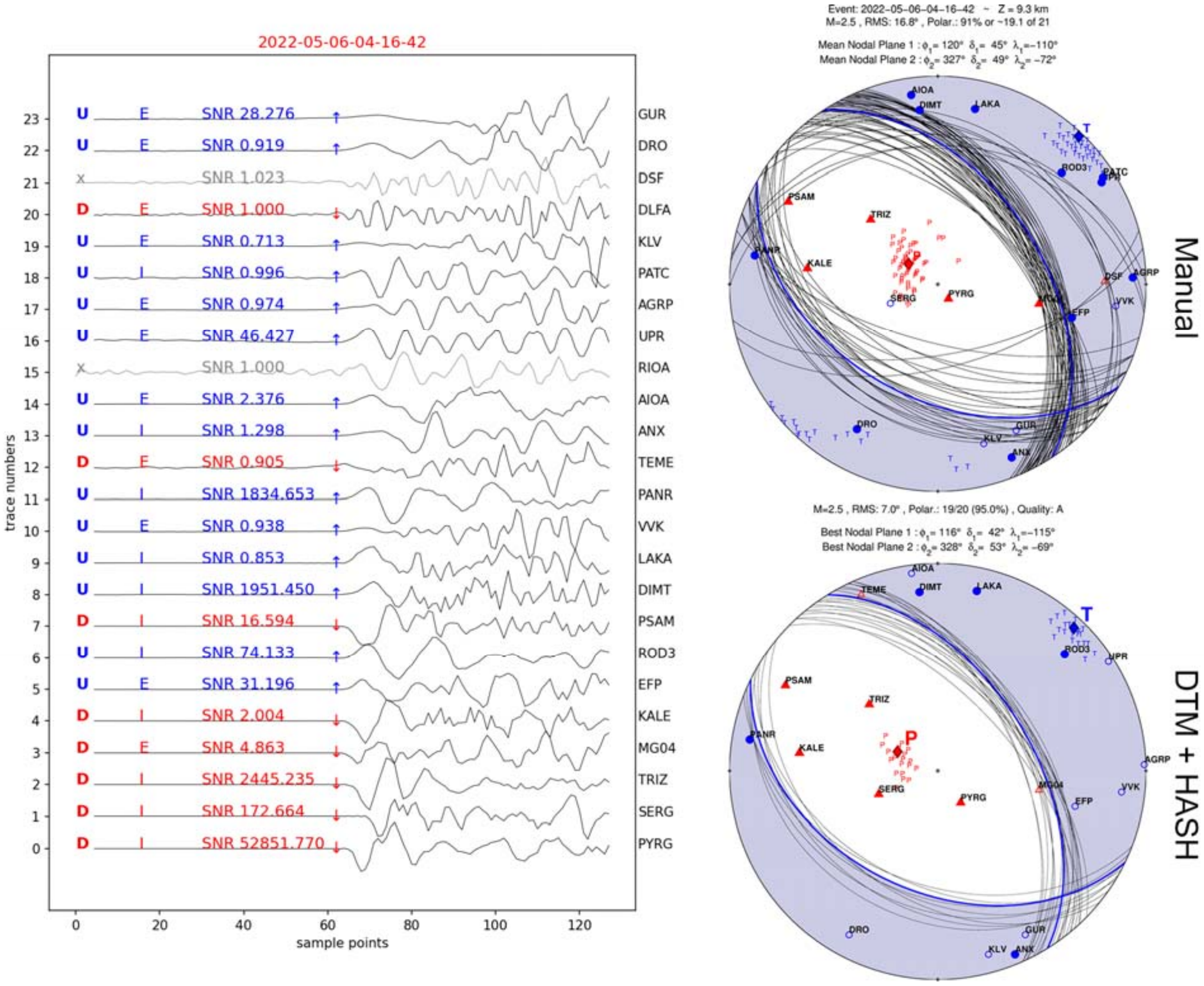

Figure 2. (Left) Example of automatic FMP measurements derived by the DiTing-Motion machine-learning model. The blue letters marked with "U" denote compression while the red letters marked with "D" denote dilatation. Gray lines (marked with "x") denote no measurement. "I" and "E" denote impulsive and emergent first motion, respectively. SNR is the Signal-to-Noise Ratio. (Right, Top) focal mechanism derived from manually measured FMPs and a grid-search over fault plane solutions that are consistent with the FMPs. (Right, Bottom) focal mechanism for the same event derived by HASH using the FMPs of the left panel. The RMS value refers to the angular difference between the best solution (bold blue nodal planes) and the valid individual fault planes (thin nodal planes). Blue circles denote compression and red triangles denote dilatation. Small red P and blue T symbols show the distribution of the P- and T-axes projections for valid individual solutions.

Results

The automated workflow yielded 370 focal mechanisms for the WGoC crisis and 65 for the aftermath period, classified by HASH with a quality grade "A". Figure 3 (left) shows a confusion matrix comparison between characterized polarities by the applied workflow and FMPs measured for the second period by Kaltsas et al. (2024), for 65 common events. The comparison shows that 82-89% of the FMPs were assessed in a similar manner both automatically and manually. Notably, however, 10-13% of FMPs were discarded by DTM. A closer examination revealed that the cases of "missed" FMPs by DTM mostly belong to either stations with accelerometric instruments, or stations at larger epicentral distances (>30 km). With the more distant stations removed from the comparison, the percentages of consistent FMP measurements rise to 87-91% and "missed" FMPs drop to 7-8% (Figure 3, right). Still, ~1% of compressional and 6% dilatational manual FMPs were characterized as being of the opposite polarity by DTM. A more detailed example is presented in Figure 4 for common events of the crisis period, where FMPs are additionally characterized as impulsive or emergent. This is a more subjective matter from the point of view of a human analyst, as an “emergent” characterization may refer to either a “gentle slope” first motion or a low-amplitude first motion, which can also be due to low SNR. DTM results show a larger percentage of agreement for impulsive FMPs than for emergent ones. A larger percentage of manually characterized “emergent” FMPs also tend to be rejected by DTM, which indicates that the classification of the ML model is generally on the more conservative side. An emergent FMP can probably be misjudged as an impulsive FMP of the same polarity, less probably as an emergent FMP of the opposite polarity, and even more rarely as an impulsive FMP of the opposite polarity.

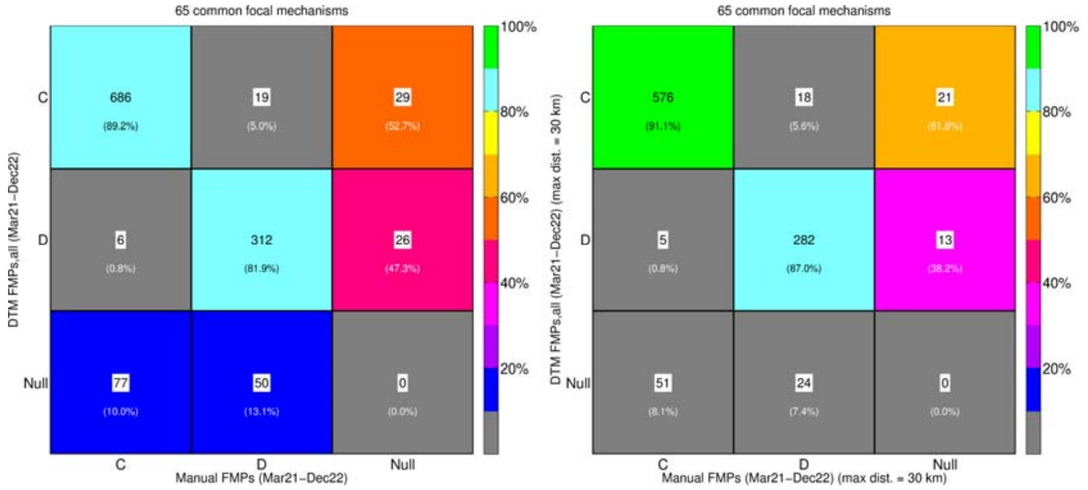

Figure 3. Confusion matrix between FMPs measured with DTM (rows) and manually (columns) for the aftermath period (March 2021 – December 2022). (Left) for all available stations, (Right) only for stations at epicentral distances < 30 km. Letters “C” and “D” denote Compression and Dilatation, respectively. The “Null” row indicates “missed” FMPs, while the “Null” column corresponds to additional automatic FMPs missing from the manual dataset.

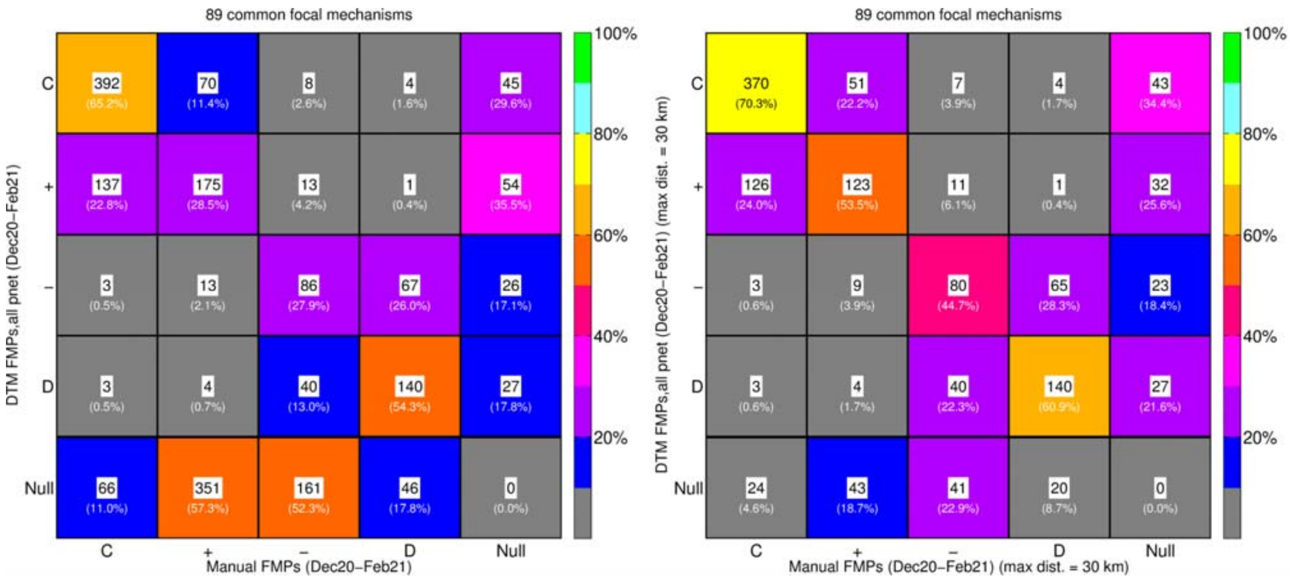

Figure 4. Same as Figure 3, but for the crisis period (December 2020 – February 2021). Symbols “+” and “-” denote emergent, whereas letters “C” and “D” denote impulsive compressional and dilatational FMPs, respectively.

A visual inspection of a subset of measured FMPs alongside the respective P-wave first pulses on the vertical component (e.g., Figure 2, left) confirmed the findings of the confusion matrices, with a generally impressive accuracy of FMP measurement in the majority of instances. There were, however, cases where the polarity of the first motion was seemingly evident to the human eye, but for some reason DTM either dismissed the measurement or misjudged the polarity. As previously noted, null measurements were mostly observed at more distant stations, where the first motion usually has a larger-period pulse than at stations near the epicenter. Erroneous DTM measurements mainly occurred in instances where the P-wave arrival-time pick was not accurate enough, which may be attributed to the applied filter during picking. We tested re-picking on the vertical component with Phasenet, retaining the P-wave pick that was found within ±1 sec of the previously available pick. When the DTM model was re-applied, some results were changed, with new FMPs added, but also with some polarities being reversed and, in some cases, previous FMP measurements being rejected. For the dataset of the 2020-2021 crisis period, the confusion matrix showed an accuracy of 89% and 80% for positive and negative polarities, respectively, taking into account stations at epicentral distances < 30 km and excluding accelerometric stations, after re-picking the P-waves with PhaseNet.

Concerning the focal mechanisms, the similarities between the solutions of the automated workflow with DTM+HASH and those with manually measured FMPs and a grid-search over all fault plane solutions that satisfy a minimum percentage of measured FMPs are quite strong (Figures 5 and 6). HASH was configured to allow for one (1) assumed erroneous FMP for each event. Most of the common solutions with a quality grade A, for both the crisis and aftermath periods, exhibit a Kagan angle of less than 30°. Larger deviations can be visibly noticed as a rotation in the focal sphere, mainly affecting the strike-slip component of the focal mechanism. Although the DTM+HASH solutions usually include fewer FMPs than the manual ones, the additional measurement of the S-to-P amplitude ratio likely helps with providing a constrained solution. However, the lack of data from some local stations, particularly for small-magnitude events, can significantly reduce the available FMPs, making the derivation of a quality grade A focal mechanism more difficult. This is especially true during the crisis period (Figure 5), as several local stations experienced technical issues that were later resolved during the aftermath period. Significant differences may also occur as the manual solutions were constrained by the addition of FMP measurements at more distant HUSN stations, where the DTM approach seems to fail to measure the FMP, as also happens sometimes at accelerometric stations due to low SNR. Figure 6 shows a comparison between 57 common solutions of manual and DTM+HASH grade A solutions for the aftermath period, indicating very similar focal mechanisms in both cases, with few notable discrepancies.

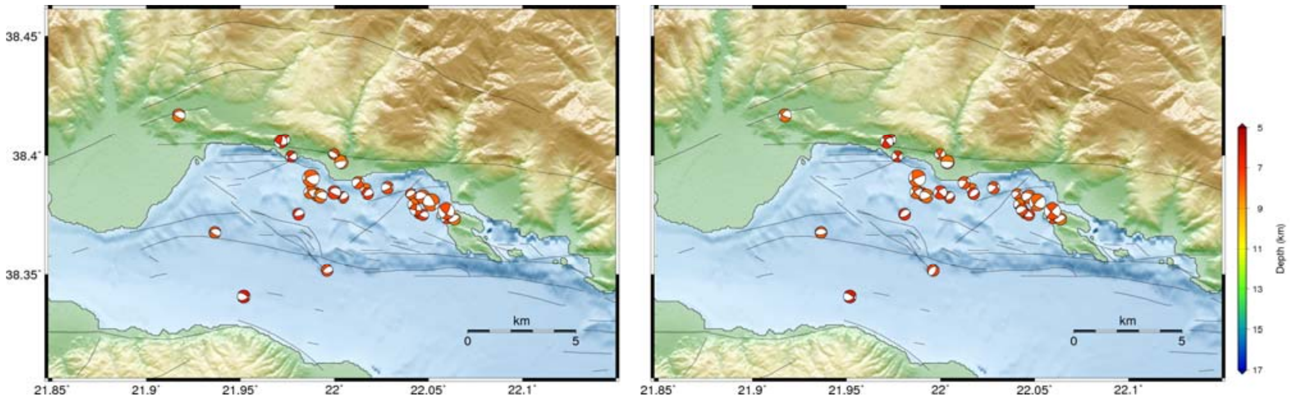

Figure 5. Focal mechanisms of 31 earthquakes during the crisis period, (Left) derived from manually determined FMPs and grid-search over adequate fault plane solutions, (Right) derived with DTM+HASH. The common events presented are those for which the DTM+HASH solutions yielded a quality grade A.

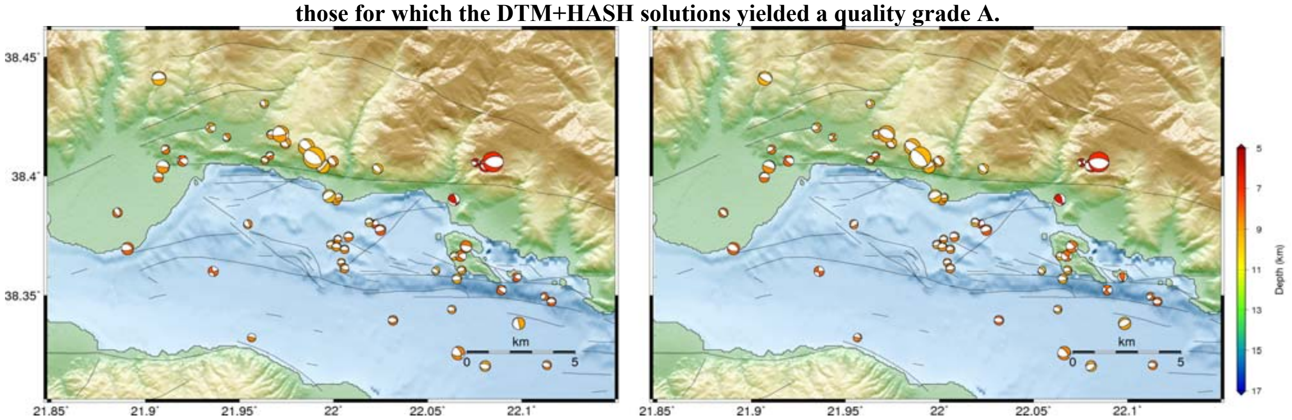

Figure 6. Same as Figure 5, but for the focal mechanisms of 57 common earthquakes during the aftermath period.

Conclusions

In this work, we showcased an application of the DiTing-Motion machine-learning model to fully automate the procedure of first motion polarity measurements in order to calculate focal mechanisms of small earthquakes in the Western Gulf of Corinth, Central Greece. As with other methods that employ artificial intelligence, this is a useful tool that can automatically extract a large amount of information that was previously unavailable. We assess the accuracy of the model to identify the polarity of the first motion and examine the cases where it rejects or produces an erroneous measurement. The method requires the availability of accurate P-wave arrival picks at local velocimetric stations for best results. With enough FMP data, even allowing for 1 or 2 erroneous measurements, an accurate focal mechanism solution can be determined. Despite the abovementioned issues, the results are still remarkable, given that they were produced with a model that was trained with a completely different dataset at a different site. As ML models can be improved by re-training, using site-specific data, this method is promising, regarding the generation of large datasets of focal mechanisms of small earthquakes. The latter could be useful for studies of fault geometries, spatial stress patterns, and even temporal stress changes prior to impending large earthquakes.

Acknowledgements

Waveform data from the following networks were used: CL (Corinth Rift Laboratory Team And RESIF Datacenter, 2013), HA (University of Athens, 2008), HP (University of Patras, 2000), HL (National Observatory of Athens, Institute of Geodynamics, Athens, 1975), and HT (Aristotle University of Thessaloniki, 1981). Maps were drawn using the Generic Mapping Tools (GMT) software (Wessel and Smith, 1998). This research is partially funded by the "TowaRds AdvaNced multidiSciplinary Fault ObseRvatory systeMs²" (TRANSFORM²) project, which is funded by the European Union under project number 101188365 within the HORIZON-INFRA-2024-DEV-01-01 call (Special Account for Research Grants of NKUA, project code: 21465).

References

Aristotle University of Thessaloniki, 1981. Aristotle University of Thessaloniki Seismological Network. International Federation of Digital Seismograph Networks. https://doi.org/10.7914/SN/HT **[Data set]**

Avallone, A., Briole, P., Agatza-Balodimou, A.M., Billiris, H., Charade, O., Mitsakaki, C., Nercessian, A., Papazissi, K., Paradissis, D., Veis, G., 2004. Analysis of eleven years of deformation measured by GPS in the Corinth Rift Laboratory area. Comptes Rendus Geosci. 336, 301–311. https://doi.org/10.1016/j.crte.2003.12.007 [**Journal Article**]

Corinth Rift Laboratory Team And RESIF Datacenter, 2013. CL - Corinth Rift Laboratory Seismological Network (CRLNET). RESIF - Réseau Sismologique et géodésique Français. https://doi.org/10.15778/RESIF.CL **[Data set]**

Chiaraluce, L., Festa, G., Bernard, P., Caracausi, A., Carluccio, I., Clinton, J.F., Di Stefano, R., Elia, L., Evangelidis, C.P., Ergintav, S., Jianu, O., Kaviris, G., Marmureanu, A., Šebela, S., Sokos, E., 2022. The Near Fault Observatory community in Europe. Annals of Geophysics 65, 3, DM316. https://doi.org/10.4401/ag-8778 [**Journal Article**]

Evangelidis, C.P., Triantafyllis, N., Samios, M., Boukouras, K., Kontakos, K., Ktenidou, O.-J., Fountoulakis, I., Kalogeras, I., Melis, N.S., Galanis, O., Papazachos, C.B., Hatzidimitriou, P., Scordilis, E., Sokos, E., Paraskevopoulos, P., Serpetsidaki, A., Kaviris, G., Kapetanidis, V., Papadimitriou, P., Voulgaris, N., Kassaras, I., Chatzopoulos, G., Makris, I., Vallianatos, F., Kostantinidou, K., Papaioannou, C., Theodoulidis, N., Margaris, B., Pilidou, S., Dimitriadis, I., Iosif, P., Manakou, M., Roumelioti, Z., Pitilakis, K., Riga, E., Drakatos, G., Kiratzi, A., Tselentis, G.-A., 2021. Seismic Waveform Data from Greece and Cyprus: Integration, Archival, and Open Access. Seismol. Res. Lett. 92, 1672–1684. https://doi.org/10.1785/0220200408 [**Journal Article**]

Ganas, A., Oikonomou, I.A., Tsimi, C., 2013. NOAfaults: a digital database for active faults in Greece. Bull. Geol. Soc. Greece 47, 518. https://doi.org/10.12681/bgsg.11079 [**Journal Article**]

Hardebeck, J.L., 2002. A New Method for Determining First-Motion Focal Mechanisms. Bull. Seismol. Soc. Am. 92, 2264–2276. https://doi.org/10.1785/0120010200 [**Journal Article**]

Hardebeck, J.L., Shearer, P.M., 2003. Using S/P amplitude ratios to constrain the focal mechanisms of small earthquakes. Bull. Seismol. Soc. Am. 93, 2434–2444. https://doi.org/10.1785/0120020236 [**Journal Article**]

Kaltsas, C., Kaviris, G., Kranis, H., Kapetanidis, V., 2024. The aftermath of the 2020-2021 seismic crisis in the Western Gulf of Corinth (Central Greece). Proceedings of 39th General Assembly of the European Seismological Commission, ESC2024-S44-622, p. 752. **[Conference Proceedings]**

Kapetanidis, V., Deschamps, A., Papadimitriou, P., Matrullo, E., Karakonstantis, A., Bozionelos, G., Kaviris, G., Serpetsidaki, A., Lyon-Caen, H., Voulgaris, N., Bernard, P., Sokos, E., Makropoulos, K., 2015. The 2013 earthquake swarm in Helike, Greece: seismic activity at the root of old normal faults. Geophys. J. Int. 202, 2044–2073. https://doi.org/10.1093/gji/ggv249 [**Journal Article**]

Kaviris, G., Elias, P., Kapetanidis, V., Serpetsidaki, A., Karakonstantis, A., Plicka, V., De Barros, L., Sokos, E., Kassaras, I., Sakkas, V., Spingos, I., Lambotte, S., Duverger, C., Lengliné, O., Evangelidis, C.P., Fountoulakis, I., Ktenidou, O.-J., Gallovič, F., Bufféral, S., Klein, E., Aissaoui, E.M., Scotti, O., Lyon-Caen, H., Rigo, A., Papadimitriou, P., Voulgaris, N., Zahradnik, J., Deschamps, A., Briole, P., Bernard, P., 2021. The Western Gulf of Corinth (Greece) 2020–2021 Seismic Crisis and Cascading Events: First Results from the Corinth Rift Laboratory Network. Seism. Rec. 1, 85–95. https://doi.org/10.1785/0320210021 [**Journal Article**]

Michelini, A., Cianetti, S., Gaviano, S., Giunchi, C., Jozinović, D., Lauciani, V., 2021. INSTANCE – the Italian seismic dataset for machine learning. Earth Syst. Sci. Data 13, 5509–5544. https://doi.org/10.5194/essd-13-5509-2021 [**Journal Article**]

Mousavi, S.M., Ellsworth, W.L., Zhu, W., Chuang, L.Y., Beroza, G.C., 2020. Earthquake transformer—an attentive deep-learning model for simultaneous earthquake detection and phase picking. Nat. Commun. 11, 3952. https://doi.org/10.1038/s41467-020-17591-w [**Journal Article**]

National Observatory of Athens, Institute of Geodynamics, Athens, 1975. National Observatory of Athens Seismic Network. International Federation of Digital Seismograph Networks. https://doi.org/10.7914/SN/HL **[Data set]**

Ross, Z.E., Meier, M., Hauksson, E., 2018. P Wave Arrival Picking and First-Motion Polarity Determination With Deep Learning. J. Geophys. Res. Solid Earth 123, 5120–5129. https://doi.org/10.1029/2017JB015251 [**Journal Article**]

Serpetsidaki, A., Kapetanidis, V., Elias, P., Rigo, A., Spingos, I., De Barros, L., Lengliné, O., Bufféral, S., Karakonstantis, A., Bernard, P., Briole, P., Zahradník, J., Kaviris, G., Plicka, V., Sokos, E., Voulgaris, N., 2023. The 2020–2021 seismic sequence in the Western Gulf of Corinth: Insights on the triggering mechanisms through high resolution seismological and geodetic data analysis. Tectonophysics 863, 230011. https://doi.org/10.1016/j.tecto.2023.230011 [**Journal Article**]

University of Athens, 2008. Hellenic Seismological Network, University of Athens, Seismological Laboratory. International Federation of Digital Seismograph Networks. https://doi.org/10.7914/SN/HA [**Data set**]

University of Patras, 2000. University of Patras, Seismological Laboratory. International Federation of Digital Seismograph Networks. https://doi.org/10.7914/SN/HP [**Data set**]

Wessel, P., Smith, W.H.F., 1998. New, improved version of generic mapping tools released. Eos, Trans. Am. Geophys. Union. https://doi.org/10.1029/98eo00426 [**Journal Article**]

Zahradnik, J., Aissaoui, E.M., Bernard, P., Briole, P., Bufferal, S., De Barros, L., Deschamps, A., Elias, P., Evangelidis, C.P., Fountoulakis, I., Gallovic, F., Kapetanidis, V., Kaviris, G., Ktenidou, O., Lambotte, S., Lengline, O., Lyon-Caen, H., Noble, M., Plicka, V., Rigo, A., Roumelioti, Z., Serpetsidaki, A., Sokos, E., Voulgaris, N., 2022. An atypical shallow Mw 5.3, 2021 earthquake in the Western Corinth Rift (Greece). J. Geophys. Res. Solid Earth 127. https://doi.org/10.1029/2022JB024221 [**Journal Article**]

Zhao, M., Xiao, Z., Zhang, M., Yang, Y., Tang, L., Chen, S., 2023. DiTingMotion: A deep-learning first-motion-polarity classifier and its application to focal mechanism inversion. Front. Earth Sci. 11. https://doi.org/10.3389/feart.2023.1103914 [**Journal Article**]

Zhu, W., Beroza, G.C., 2019. PhaseNet: A deep-neural-network-based seismic arrival-time picking method. Geophys. J. Int. 216, 261–273. https://doi.org/10.1093/gji/ggy423 [**Journal Article**]